

Tsunami-Seabed-Structure Interaction from Geotechnical and Hydrodynamic Perspectives

S. Sassa

Port and Airport Research Institute, Yokosuka, Japan

E-mail: sassa@ipc.pari.go.jp

ABSTRACT: The paper reports some recent research advances on tsunami-seabed-structure interaction following the 2011 off the Pacific Coast of Tohoku Earthquake Tsunami, Japan. It presents a concise review of the latest research performed on the stability of breakwater foundation under tsunami by utilizing a geotechnical centrifuge and a large-scale hydro flume at Port and Airport Research Institute. I highlight here the role of tsunami-induced seepage in piping/boiling, erosion and bearing capacity decrease and failure of the rubble/seabed foundation. A comparison and discussion are made on the stability assessment for the design of tsunami-resistant structures on the basis of the results from both geo-centrifuge and large-scale hydrodynamic experiments.

KEYWORDS: Breakwaters, Geo-centrifuge, Large-scale hydro flume, Seepage, Tsunami

1. INTRODUCTION

The 2011 off the Pacific Coast of Tohoku earthquake tsunami devastated the eastern part of Japan and caused significant damages and destroyed the breakwaters. Several tsunami-induced forces acted on the breakwaters with reference to Figure 1a. Among these forces, the water level difference between inside and outside of the caissons gave rise to a long-duration seepage flow in the foundations. Although the concrete mechanisms responsible for the breakwater failures remain to be determined, the instability of the breakwater foundations under tsunami should be one of the key factors affecting the failure of the structures resting on the rubble/seabed foundations.

Here, I highlight the role of seepage in the context of tsunami-seabed-structure interactions, from geotechnical and hydrodynamic perspectives. Particular focus will be placed on the occurrence of piping/boiling, erosion and bearing capacity decrease and failure of the rubble/seabed foundations (Figure 1b). Indeed, the paper reviews and summarizes the essential results obtained through the use of a geotechnical centrifuge and a large-scale hydro flume at Port and Airport Research Institute (Takahashi et al., 2013, 2014; Arikawa and Shimosako, 2013, Arikawa et al., 2013). Both results will be compared and discussed in view of the rational stability assessment and design of tsunami-resistant caisson breakwaters with rubble foundations.

2. GEO-CENTRIFUGE STUDY

It is essential to reproduce a prototype-scale stress field in clarifying the instability of breakwater foundations under tsunami. Geo-centrifuge makes it possible and has proven effective in studying fluid-soil interaction problems (Sassa and Sekiguchi, 1999). Here, I report our novel use of geo-centrifuge for studying tsunami-seabed-structure interaction involving the role of tsunami-induced seepage (Takahashi et al., 2013, 2014). A notable difference from the previous study is that the seepage flow in the rubble mound becomes turbulent due to the high permeability of the mound as crushed rocks. The similitude for such turbulent seepage flow will first be discussed in comparison to the viscous scaling that has been used to satisfy the similitude for laminar seepage flow in a geo-centrifuge.

2.1 Similitude for tsunami-induced seepage flow in rubble mounds

Suppose that a centrifuge tsunami test with a 1/N scaled model is performed under a steady-state centrifugal acceleration of Ng, where N is the scale factor and g represents the acceleration due to the Earth's gravity. According to the Dupuit - Forchheimer's

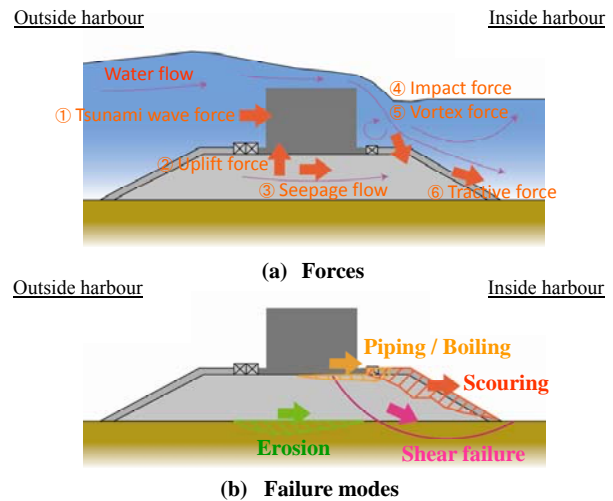


Figure 1 Tsunami-induced forces on caisson breakwaters and failure modes of the foundation. (Descriptions are added to Figure 1 of Takahashi et al. (2014))

approximation, the relationship between the hydraulic gradient i and mean seepage flow velocity \bar{v} can be expressed as

$$i = a\bar{v} + b\bar{v}^2 \quad (1)$$

$$a = \alpha_0 \frac{\mu (1-n)^3}{Ng n^2 d_{15}^2} \quad b = \beta_0 \frac{1-n}{Ng n^2 d_{15}} \quad (2)$$

Here, α_0 and β_0 are coefficients, μ is the dynamic viscosity of the pore fluid, n is the porosity of the ground, d_{15} is the grain size passing 15% finer by weight. The hydraulic gradients in horizontal and vertical directions can be written as

$$i_x = \frac{1}{\gamma_w} \frac{\partial \Delta u}{\partial x} = \frac{1}{\rho Ng} \frac{\partial \Delta u}{\partial x} \quad (3)$$

$$i_y = \frac{1}{\gamma_w} \frac{\partial \Delta u}{\partial y} = \frac{1}{\rho Ng} \frac{\partial \Delta u}{\partial y} \quad (4)$$

where Δu is the excess pore water pressure, γ_w is the unit weight of the fluid, and ρ is the mass density of the fluid.

In the laminar flow regime, the viscous term, i.e. the first term of the right-hand side of Eq. (1), becomes dominant. For such Darcy flow, the associated similitude can be fulfilled by using viscous fluid

whose dynamic viscosity is N times that of water, with the hydraulic gradient and mean flow velocity as equivalent with those of the corresponding prototype (Eqs. (2)-(4), Table 1). With this technique, called viscous scaling, one can satisfy the time-scaling laws for fluid wave propagation and the consolidation of the soil (Sassa and Sekiguchi, 1999). By contrast, in the turbulent flow regime, the inertia term, i.e. the second term of the right-hand side of Eq. (1), becomes dominant, for which one can satisfy the associated similitude by using the $1/N$ scaled grain diameter, with the equivalent hydraulic gradient and mean flow velocity as those of the corresponding prototype (Eqs. (2)-(4), Table 1). It should be noted that the Reynolds number which may be important in turbulent solitary wave boundary layers (Sumer et al., 2010), is not scaled here, because the present purpose is to reproduce the distributions of pore water pressure and mean seepage flow velocity, thereby clarifying the effect of the seepage force on the stability of breakwater foundations.

Table 1 Comparison of similitudes for laminar and turbulent seepage flows in a geo-centrifuge

	Similarity ratio		
	Prototype	Present study**	Viscous scaling*
g	1	N	N
Size	1	$1/N$	$1/N$
Grain size	1	$1/N$	1
Dynamic viscosity	1	1	N
Pressure, Stress	1	1	1
Hydraulic gradient	1	1	1
a^* or b^{**} in Eq. (1)	1	1	1
Mean flow velocity	1	1	1

* Laminar flow case, ** Turbulent flow case

2.2 Experiment model

The experiment models represent those of the Omaezaki breakwater and the Kamaishi breakwater in Japan. Their photographs are shown in Figure 2, together with the close-up of the mound materials used. Note here that the Omaezaki model was tested under 50g with the corresponding 60m-prototype width, while the Kamaishi model was tested under 75g with the corresponding 90m-prototype width, as shown in Figure 2.

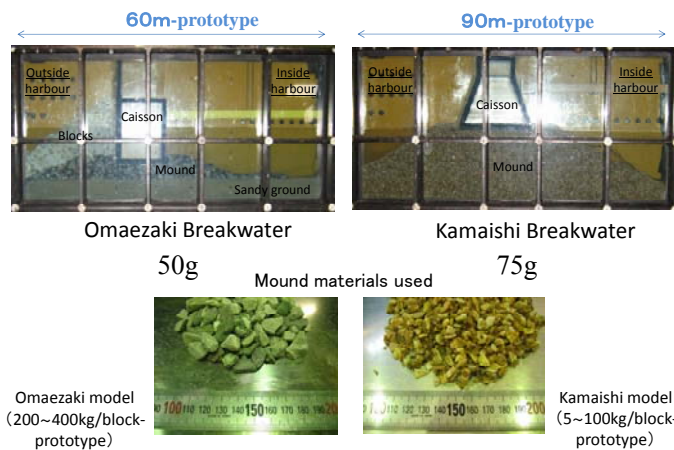
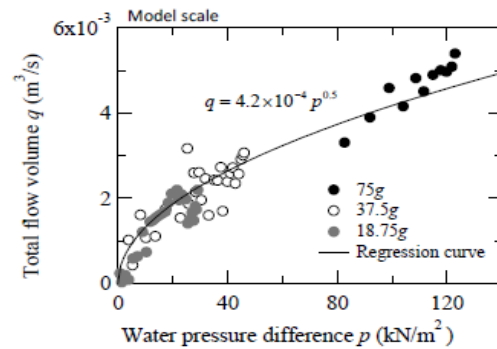
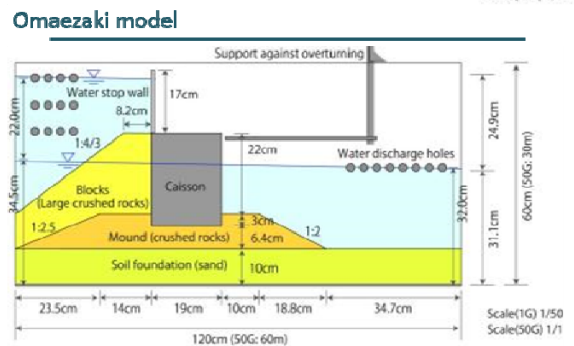
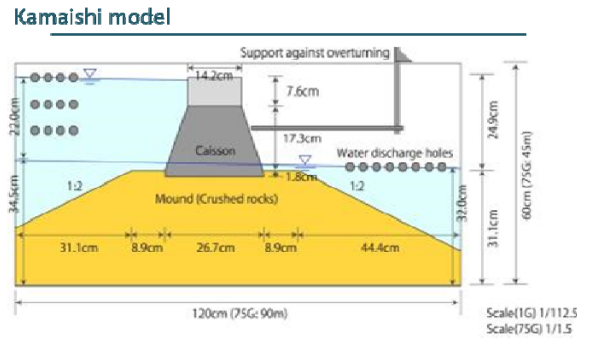
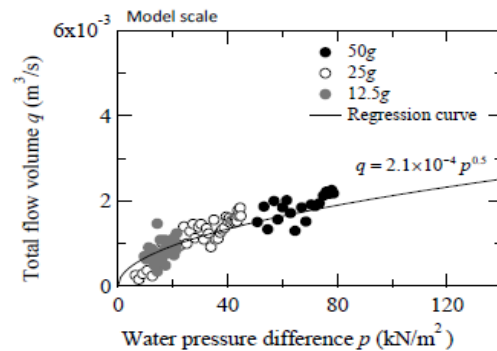


Figure 2 Experiment models used for the geo-centrifuge study

Water was supplied under a given steady state centrifugal acceleration where the targeted water level difference was set-up and maintained throughout the course of the experiment (Figure 3). The relationships between the water pressure difference p and the seepage flow volume q through the mound that were measured under different gravities (Figure 3a,b), show that q was proportional to a root of p , indicating that the seepage flow in the mound was indeed turbulent according to Eq. (1) described above.



(a) Kamaishi model (Rock A)



(b) Omaezaki model (Rock B)

Figure 3 Verification of turbulent seepage flow field in a geo-centrifuge. (Figure 5a,b and Figure B1 of Takahashi et al. (2014) are combined)

The role of such tsunami-induced turbulent seepage in piping/boiling, erosion and bearing capacity decrease and failure of caisson breakwaters will be summarized below, on the basis of our experimental and numerical work reported in Takahashi et al. (2014).

2.3 Piping/boiling

The occurrence of piping and boiling was tested against the Omaezaki and Kamaishi models described above. The tsunami-induced water level differences were set at 8m on prototype scale for the Omaezaki model and at 16m for the Kamaishi model. Both conditions correspond to severest possible conditions in the field. The experimental results show that the piping and boiling did not take place. The hydraulic gradients induced underneath the caissons were $i = 0.4$ for the Omaezaki model and $i = 0.6$ for the Kamaishi model (Figure 4). On the basis of these results, a deformed Omaezaki model was also tested, and light boiling was observed to occur in this model (Figure 4). The value of i underneath the caisson was as high as 1.1. This result is consistent with theory in soil mechanics such that boiling typically occurs when $i > 1.0$.

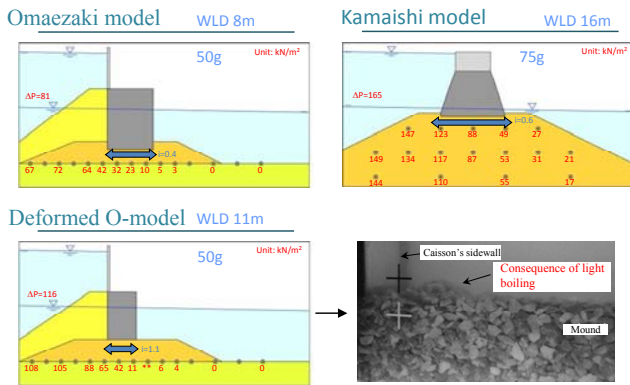


Figure 4 Pressure distributions in three different models. (Descriptions are added to Figure 8 and Figure 9b of Takahashi et al. (2014). Boiling was observed to occur in the deformed O-model)

2.4 Seepage erosion

Tsunami-induced seepage can induce erosion in a sandy ground underneath the rubble mound of caisson breakwaters. Experiments were performed under conditions where no sliding and/or overturning of the caisson was allowed to occur in order to focus on the erosion process of the sandy ground. The experimental results on the Omaezaki model show that such seepage erosion progressed with time at the vicinity of the rubble/sand interface (Figure 5). The eroded mass deposited in the onshore side of the mound in accordance with the onshore direction of the seepage flow. Accordingly, the caisson settled as a consequence of the tsunami-induced seepage erosion.

2.5 Bearing capacity decrease and failure

The bearing capacity decrease and failure characteristics of the rubble mounds of caissons were examined using the model cross-sections shown in Figure 6. In order to control the horizontal loading toward the caisson and the seepage flow caused by tsunami independently, a vertical water stop wall was installed. It may be important here to note that the seepage direction was rather oriented upward with this treatment than that in the actual situations in the field, and this aspect of the behavior will be referred to later in this paper. Also, the caisson with drainage holes at the bottom was used to eliminate the effect of the uplift force on the caisson and to focus on the effect of the tsunami-induced seepage on the bearing capacity of the mound. The results of the horizontal loading test show that the deformed area was concentrated on the top shoulder of the

mound, indicating the occurrence of strain localization in the limit state (Figure 6). The results of the combined horizontal loading and seepage flow test show that a bearing capacity failure took place, accompanying flow deformations of the mound (Figure 7). The hydraulic gradient induced around the top shoulder of the mound was equal to $i = 0.4$ in the Model B (Figure 6). Note here that the failure did not take place under the same load without the seepage. In fact, the measured relationships between the horizontal load and displacement show that the bearing capacity of the mound decreased by approximately 30% due to the tsunami-induced seepage (Figure 7).

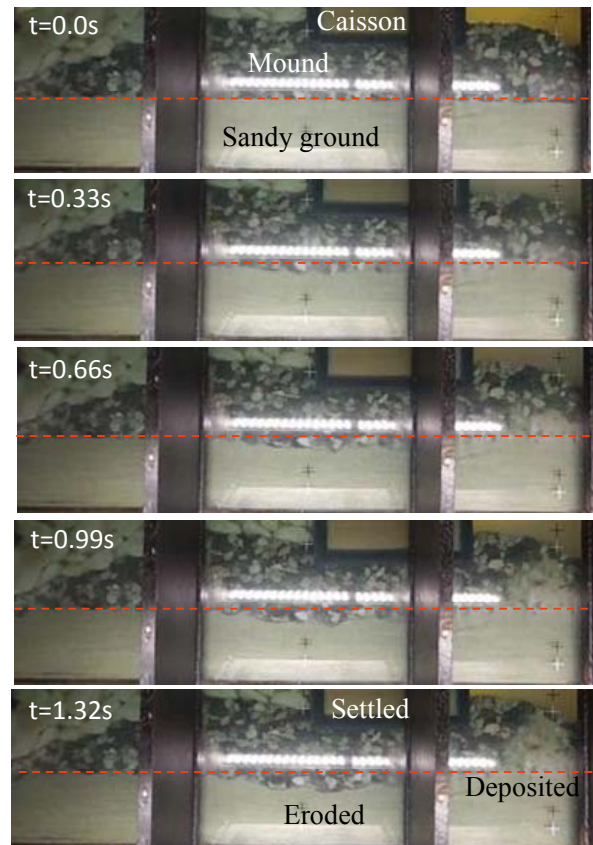
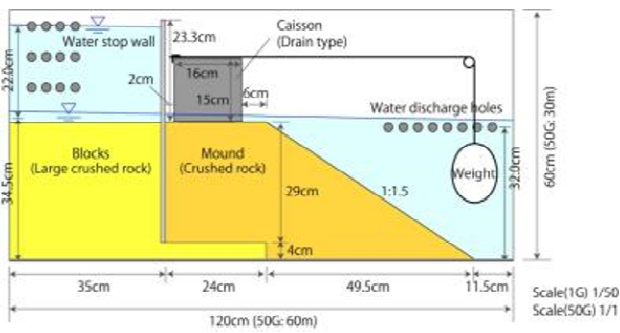


Figure 5 Progress of seepage erosion. (Descriptions are added to Figure 7 of Takahashi et al. (2014). Settlement of the caisson was observed to occur with seepage erosion)

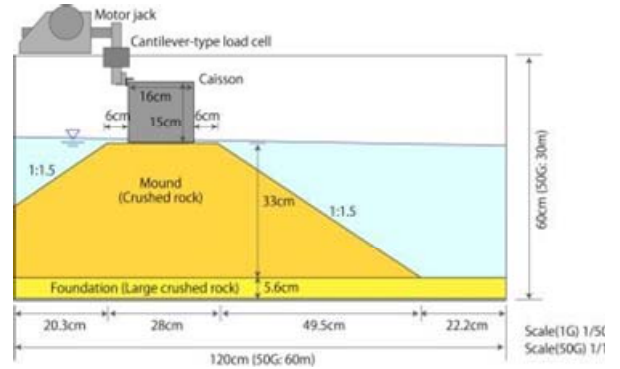
In order to confirm the above experimental finding and extend the knowledge to actual field conditions, the finite element analysis was conducted using the GeoFEM code developed at Port and Airport Research Institute. Although the seepage flow in the mound was turbulent, the analysis assumed Darcy flow adopting the linear relationship between the seepage flow velocity and the hydraulic gradient. As such, the material parameters involving the permeability coefficient were selected so as to yield the measured hydraulic gradient ($i = 0.4$) in the top shoulder of the mounds, whose region proved to be important in light of the stability of the caisson. The numerical results show that the excess pore water pressure distributions, the deformation characteristics, and the decrease in the bearing capacity as measured in the experiments were adequately reproduced by the analysis (Figure 8).

On the basis of the above results, we analyzed the generalized cross sections concerning the commonly used caisson breakwaters in Japan, i.e. caisson width 10m and height 12m (Figure 9). Recall here that the seepage direction was rather oriented upward in the experiment, but, actually is diagonal toward the slope of the mound as is the case here. The analysis adopted the horizontal loading,

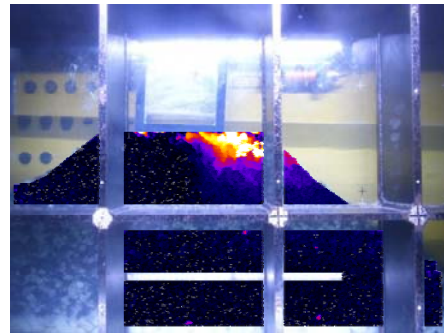
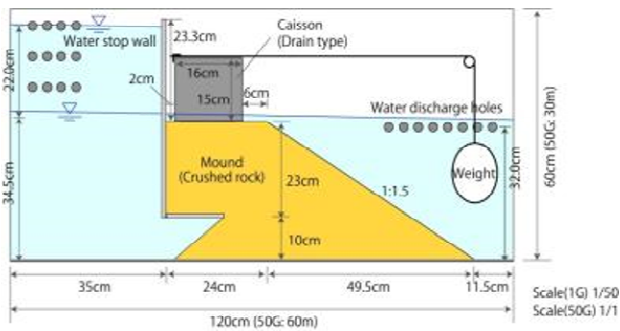
Model A



Horizontal loading test



Model B



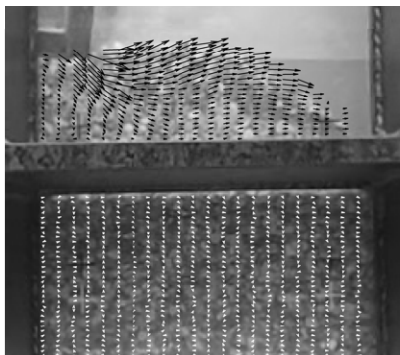
Deformed area

Figure 6 Model cross-sections used for clarifying the bearing capacity characteristics of rubble mounds of caissons. (Figure 11 and Figure 13a of Takahashi et al. (2014) are combined. Deformed area is marked in red color)

Horizontal loading + Seepage flow (model B)



Bearing capacity failure



Displacement vectors of the mound

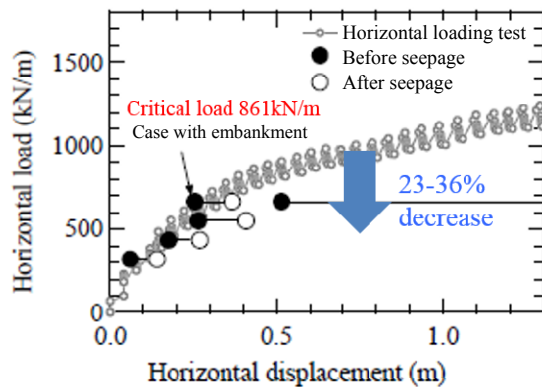
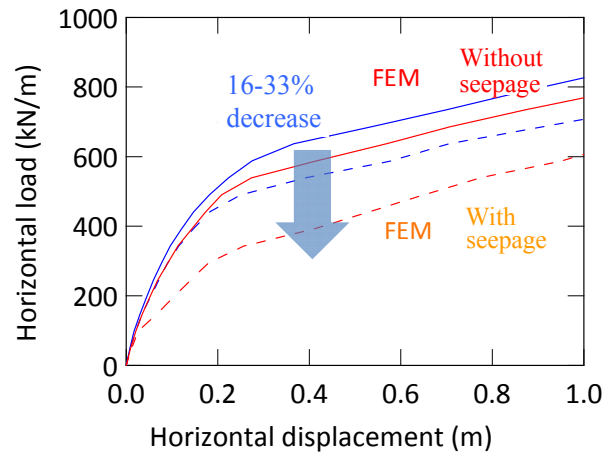
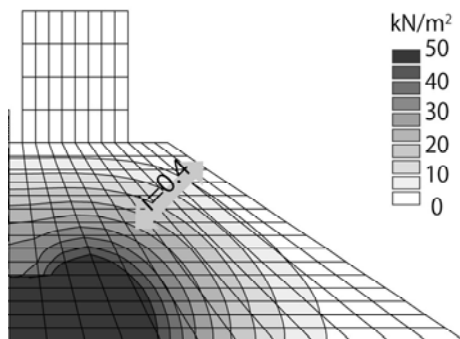


Figure 7 Seepage-flow induced bearing capacity failure. (Figure 16b and Figure 17 of Takahashi et al. (2014) are combined and descriptions are added)



Excess pore pressure distributions



Deformation distributions

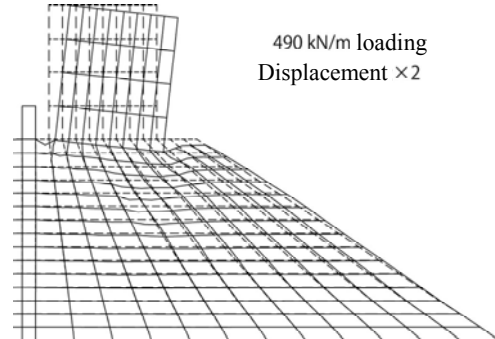
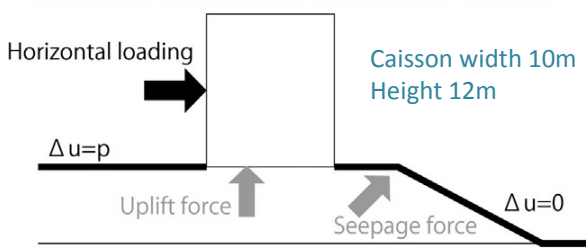


Figure 8 FEM analysis for reproduction: Pressure/Deformation distributions/Bearing capacity. (Figure 19b, Figure 20 and Figure 21b. of Takahashi et al. (2014) are combined and descriptions are added. The blue and red lines denote analyses with and without cohesion.)

Concept for boundary/loading conditions

Horizontal loading + Uplift force + Seepage force



Horizontal loading + Uplift force

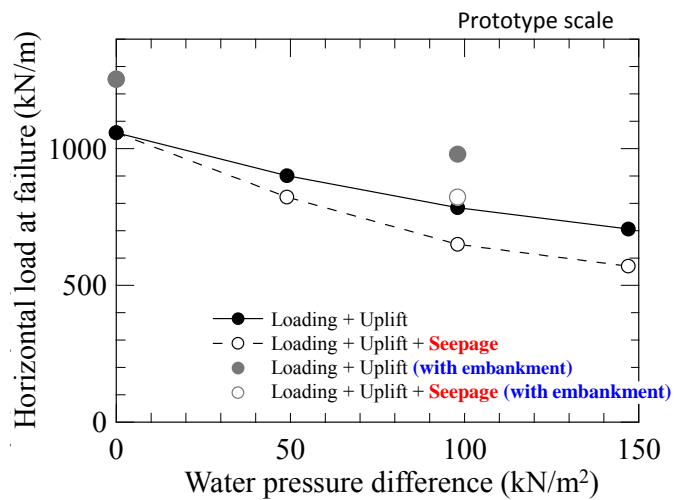
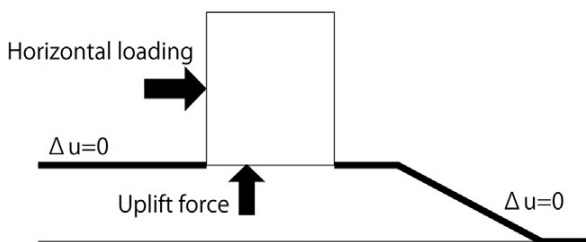


Figure 9 Analysis of generalized cross sections. (Figure 23 and Figure 26 of Takahashi et al. (2014) are combined and descriptions are added)

uplift force and seepage force independently, so as to elucidate the effect of the seepage on the bearing capacity of the mound. The numerical results show that the seepage effect became more pronounced with increasing water pressure (level) differences (Figure 9). For instance, a water level difference of 10m, i.e. water pressure difference 98kN/m^2 gave rise to the decrease of the bearing capacity by 20% owing to the tsunami-induced seepage. The influence of placing a surcharge embankment as countermeasures was also examined. The embankment as thick as 2m had a certain effect on improving the bearing capacity of the caisson breakwaters (Figure 9).

3. LARGE-SCALE HYDRO FLUME STUDY AND DISCUSSION

This section discusses a large-scale hydro flume study performed by Arikawa et al. (2013), in light of the geo-centrifuge study described above. For this purpose, I focus on the bearing capacity failure of caisson breakwaters. The hydro flume used was 184m long and 3.5m wide and 12m deep. Arikawa et al. (2013) modeled the Omaezaki breakwater with a 1/7.5 scaled model that was 40.98kN/m and 1.5m thick. With reference to Figure 10, dummy caissons which were 10% heavier per 1m of width than the model caisson were installed at both ends of the channel. Water was discharged from the offshore side gate and taken in the shore side gate of the flume, creating a water level difference between outside

and inside of the caisson. The modeled water level difference was 4.5m on prototype scale. In order to prevent the occurrence of erosion of the sandy ground, a thin concrete plate was installed just underneath the rubble mound (Figure 10). The experimental results show that the bearing capacity failure took place accompanying flow deformations of the mound (Figure 10).

In the design of caisson breakwaters in Japan, the safety against sliding, overturning and bearing capacity failure needs to be clarified and assured according to the Technical Standard for Port and Harbour Facilities with Commentary. Conventional slip-circle Bishop analysis has been used to calculate the safety factor for the bearing capacity of the mound. It is important here to remark that the safety factor for the bearing capacity calculated by Arikawa et al. (2013) for the above hydro flume experiment was higher than unity, whose discrepancy with the actual caisson failure was of the order of 10%. This appreciable discrepancy can be explained as follows. Namely, the geo-centrifuge study combined with the numerical analysis has shown that the bearing capacity decreased essentially linearly with increasing water level difference due to the effect of the tsunami-induced seepage. As a consequence, the water level difference of 4.5m as modelled in the large-scale hydro flume experiment yielded the bearing capacity decrease of approximately 10% in Figure 9. This quantitative agreement is noteworthy considering the two distinctly different approaches from both geotechnical and hydrodynamic perspectives.



Figure 10 Large-scale hydro flume experiment of Arikawa and Shimosako (2013), showing views before and after the experiment. Caisson failed accompanying flow deformations of the rubble mound under tsunami

4. CONCLUSIONS

The paper has summarized some recent research advances on tsunami-seabed-structure interaction through the use of the geo-centrifuge and large-scale hydro flume at Port and Airport Research Institute, with particular focus on the role of tsunami-induced seepage in the piping/boiling, erosion and bearing capacity decrease and failure of caisson breakwaters. I discussed the similitudes for laminar and turbulent seepage flows in a geo-centrifuge, and have shown that the viscous scaling, which has successfully been used for studying wave-soil interaction problems, can be replaced by the similitude for turbulent seepage flow in studying the stability of rubble mound foundations under tsunami. Notably, both geo-centrifuge and large-scale hydro flume experiments proved to be consistent with each other, based on the role of the tsunami-induced seepage in the bearing capacity failure of caisson breakwaters. This provides good support for both approaches to tsunami-seabed-structure interaction problems. Accordingly, the role of such tsunami-induced seepage should be taken into account in the future design practice in order to facilitate the rational stability assessment of tsunami-resistant caisson breakwaters with rubble foundations.

5. REFERENCES

- Arikawa, T. and Shimosako, K. (2013) "Failure mechanism of breakwaters due to tsunami: a consideration to the resiliency", Proceedings of 6th Civil Engineering Conference in the Asian Region, Jakarta, Indonesia, pp1-8.
- Arikawa, T., Sato, M., Shimosako, K., Tomita, T., Yeom, G.-S., and Niwa, T. (2013) "Failure mechanism and resiliency of breakwaters under tsunami", Technical Note of the Port and Airport Research Institute, No. 1269, pp1-37 (in Japanese).
- Sassa S., and Sekiguchi, S. (1999) "Wave-induced liquefaction of beds of sand in a centrifuge", Géotechnique, 49, No.5, pp 621-638.
- Sumer, B. M., Jensen, P. M., Sorensen, L. B., Fresoe, J., Liu, P. L.-F. and Carstensen, S. (2010) "Coherent structures in wave boundary layers: Part 2. Solitary motion", Journal of Fluid Mechanics, 646, pp207-231.
- Takahashi, H., Sassa, S., Morikawa, Y. and Takano, D. (2013) "Stability of breakwater foundation under seepage flow caused by tsunami", Report of the Port and Airport Research Institute, 52, No.2, pp3-23 (in Japanese).
- Takahashi, H., Sassa, S., Morikawa, Y., Takano, D. and Maruyama, K. (2014) "Stability of caisson-type breakwater foundation under tsunami-induced seepage", Soils and Foundations, 54, doi: 10.1016/j.sandf.2014.07.002.